PAPER

Check for updates

Stepwise post-synthetic linker installation in rare-earth metal–organic frameworks†

Yuchen Hu,[a] Rebecca Shu Hui Khoo,[b] Aiying Pang,*[c] Sizhuo Yang,[b] Christian Fiankor, [ID][a] Xu Zhang*[c] and Jian Zhang [ID] *[b]

Metal–organic frameworks based on rare earth elements (*i.e.* RE-MOFs) represent an important class of porous crystalline materials that have gained increasing attention due to their diverse optical, photophysical, and electronic properties. Developing strategies to enrich their properties is of great interest to expand their applications. Post-synthetic installation of secondary linkers to RE-MOFs, in principle, is an effective approach to incorporate new functionalities of RE-MOFs. However, the lack of synthesis control to generate RE-MOFs that consist of less connected clusters for linker installation limits the utility of this methodology. Herein, a co-modulator strategy was successfully used to synthesize RE-MOFs consisting of 8-connected RE_6 clusters with **scu** topology. These new RE-MOFs allow the precise installation of different secondary linkers including photosensitizers along the *a* and *c* crystallographic axes *via* single-crystal-to-single-crystal transformation, and the resulting RE-MOFs exhibit either enhanced or inhibited energy transfer depending on the energy level of the inserted linker. Our work provides an effective approach for the design and synthesis of multifunctional RE-MOFs.

1. Introduction

During the evolution of reticular chemistry in the past two decades, the employment of polynuclear clusters as secondary building units (SBUs) to construct metal–organic frameworks (MOFs) marks a distinct turning point.[1] Compared with the conventional single-metal nodes, SBUs allow for the directional assembly of stable crystalline porous materials, which significantly expands the applications of MOFs.[2] One outstanding example is zirconium MOFs (Zr-MOFs) that are mostly based on hexanuclear $[Zr_6(\mu_3\text{-}O)_4(\mu_3\text{-}OH)_4]$ (Zr_6) clusters. The exceptional adaptability of Zr_6 clusters promotes a diverse connectivity based on the carboxylic ligands with various geometries. To date, Zr_6 clusters serving as 4-, 6-, 8-, 9-, 10-, and 12-connected SBUs have been documented.[3,4] In particular, the less connected

clusters offer an efficient platform to modify Zr-MOFs *via* postsynthetic linker installation to place multiple functional groups into predetermined positions with atomic level precision.[5–7]

Recently, MOFs based on rare-earth (RE) elements (*i.e.*, RE-MOFs) have received increasing attention due to their unique optical, magnetic, and electronic properties, in addition to the conventional applications in gas storage and separation.[8–15] Compared with the widely studied Zr-MOFs, RE-MOFs share some topological similarities, of which the prominent one being that the **fcu** topology can be found in both frameworks when linking Zr_6 and RE_6 clusters with ditopic ligands, respectively.[3,16] Nonetheless, some major difference between Zr-MOFs and RE-MOFs does exist because the hard-sphere behavior and relatively large size of the RE cations allow for multiple directionalities of coordinated carboxylic ligands.[17] Typically, each RE cation can coordinate with 6 to 12 terminal ligands, while each Zr^{4+} can only coordinate with eight. The higher coordination number along with the moderate RE–O bond strength gives rise to a large library of unique polynuclear RE clusters that lead to the formation of sophisticated RE-MOFs with fascinating topologies.[18–23] Indeed, many highly adaptable RE_4, RE_6, RE_9, and RE_{18} clusters, some of which are difficult to access with other metals, have been discovered as building blocks for the assembly of RE-MOFs with diverse topologies and high connectivity.[24–27] It should be noted, however, the formation and stabilization of several polynuclear clusters in RE-MOFs were recently found to be facilitated by the bridging F^- ions that are generated *in situ* during materials synthesis from the decomposition of modulators such as 2-fluorobenzoic acid.[28,29]

[a] Department of Chemistry, University of Nebraska-Lincoln, Lincoln, Nebraska 68588, USA

[b] The Molecular Foundry, Lawrence Berkeley National Laboratory, Berkeley, California 94720, USA. E-mail: jianzhang@lbl.gov

[c] School of Chemistry and Chemical Engineering, Huaiyin Normal University, Jiangsu Engineering Laboratory for Environment Functional Materials, Jiangsu Collaborative Innovation Center of Regional Modern Agriculture & Environmental Protection, No. 111 West Changjiang Road, Huaian, Jiangsu 223300, China. E-mail: ayp@hytc.edu.cn, zhangxu@hytc.edu.cn

† Electronic supplementary information (ESI) available: Synthesis, experimental details and procedures, NMR spectra, crystallographic information, SEM and EDX analysis, PXRD patterns, acid digestion experiments, UV-vis absorption and emission spectra, luminescence lifetime trace, phosphorescence spectra are appended. CCDC 2308004–2308010. For ESI and crystallographic data in CIF or other electronic format see DOI: https://doi.org/10.1039/d3tc04365g

On the other hand, although post-synthetic linker installation has proven to be an effective strategy to construct multi-component Zr-MOFs,[30–37] it is not straightforward to apply this method to increase the structural complexity and enrich the functionality of RE-MOFs. This is because that it is often challenging to synthesize RE-MOFs consisting of less connected polynuclear clusters, the required framework component to install secondary linkers. For example, the combination of Zr^{4+} with square-shaped tetratopic linkers usually form **ftw** or **shp** nets based on 12-connected Zr_6 clusters.[38–44] By using rectangular linkers with high aspect ratio, Zr-MOFs with reduced SBU connectivity, such as 8-, 6-, and 4-connected Zr_6 clusters, can be constructed with **scu/csq/sqc**, **soc**, and **lvt** topology, respectively.[3] Unfortunately, this ligand symmetry reduction strategy often appears ineffective for RE-MOFs,[45–48] likely because the less connected RE clusters inevitably destabilize during MOFs growth and lead to the formation of other thermodynamically favored products with fully connected SBUs.[49–51]

Thus, despite some recent success involving major modification of the main ligand such as desymmetrization of tetra-carboxylate linkers, synthetic approaches to construct RE-MOFs consisting less connected clusters are not widely available.[52–54] Therefore, developing simple strategies to reduce the connectivity to allow for multifunctionality installation in RE-MOFs is highly desirable. The unsaturated metal sites within less connected clusters can offer the binding site to install secondary linkers that can not only increase the stability but also introduce new functions into the pristine RE-MOFs. Herein, we report the design and synthesis of RE-MOFs with 4,8-connected **scu** topology, NPF-320-RE (RE = Eu, Tb; NPF = Nebraska Porous Framework). This is achieved *via* a straightforward co-modulator method for the MOFs synthesis, and the resulting framework materials NPF-320-RE are indeed capable to incorporate different secondary linkers into distinct location. Furthermore, we show that two photosensitizer-based ditopic secondary linkers can be installed in a stepwise fashion in the framework along different crystallographic axes *via* single-crystal-to-single-crystal transformation. Overall, our work offers another approach to enhance and control the luminescent properties of RE-MOFs.

2. Experimental

2.1 Materials and methods

All solvents and reagents were purchased from commercial suppliers and, unless otherwise noted, used without further purification. Solution ^{1}H and ^{13}C nuclear magnetic resonance NMR measurements were performed on a Bruker FT-NMR spectrometer (400 MHz) or a Bruker FT-NMR spectrometer (300 MHz). Mass spectra (MS) were performed on a Waters Q-TOF mass spectrometer. Powder X-ray diffraction (PXRD) patterns were taken with either a PANalytical Empyrean diffractometer with a PIXcel 3D detector and a Rigaku Miniflex 6G XRD. The copper target X-ray tube was set to 45 kV and 40 mA.

Scanning Electron Microscope. SEM images and EDS data were collected on a tabletop Phenom ProX equipped with the Element Identification (EID) software package and a specially designed and fully integrated Energy Dispersive Spectrometer (EDS).

Photoluminescence and excitation spectra were measured on a PerkinElmer LS55 spectrometer. UV-vis spectra were measured using an Agilent Cary 300 UV-vis spectrometer. Fluorescence lifetimes were measured on an Edinburgh FLS1000 spectrometer with an EPLED-365 light source. Well suspended samples of NPF-320-RE ($\sim$5 mg) in DMF were used photoluminescence tests.

Acid digestion was performed in 500 μL DMSO-d_6 with 25 μL D_2SO_4 at 60 °C until the solution get clear, then the solution was used for ^{1}H NMR measurement.

2.2 Synthetic procedures

Tetratopic ligand **H₄L** was synthesized *via* the typical Suzuki couplings followed by saponification in a basic aqueous solution. Detailed synthesis procedure of **H₄L** has been reported in the literature.[55] Ditopic secondary linker 9*H*-carbazole-2,7-dicarboxylic acid (**CzDC**) was purchased and used without purification. The synthesis of ditopic secondary linker carbazole-substituted terphenyl dicarboxylic acid (**CzTPDC**) was described in detail in ESI† (Fig. S1).

Synthesis of NPF-320-Eu. Eu(NO₃)₃·6H₂O (3 mg) and 2-fluo-robenzoic acid (2-FBA, 150 mg) were mixed in 1 mL DMF in a glass vial and ultrasonically dissolved. The clear solution was heated in an oven at 80 °C for 1 h. After cooling down to room temperature ligand **H₄L** (3 mg) and 10 μL trifluoroacetic acid (TFA) were added to this solution and the mixture was sonicated for 5 min to dissolve all ligand. Then the yellow solution was put into an oven and the temperature was increased from 30 °C to 115 °C in 2 h and then kept at 115 °C for 48 h. After cooling down to room temperature in 2 h, needle-shaped single crystals were obtained. After activation, the samples were washed with fresh DMF and stay in DMF for further use.

Synthesis of NPF-320-Tb. NPF-320-Tb was synthesized in the similar procedure as that of NPF-320-Eu, except for the use of Tb(NO₃)₃·6H₂O (3 mg) as the metal source.

Post-synthetic installation of secondary linkers in NPF-320-RE. NPF-320-RE (RE = Eu or Tb, $\sim$4 mg) was soaked in 1 mL DMF solution of secondary linker (biphenyl-4,4′-dicarboxylic acid (**SL₁**), 2′,5′-dimethyl-[1,1′:4′,1″-terphenyl]-4,4″-dicarboxylic acid (**SL₂**), **CzDC**, or **CzTPDC**, 3.3 μmol). The sample was then put in oven and the temperature was increased from 30 °C to 60 °C in 2 h and then kept at 60 °C for 12 h. After cooled down to room temperature, the solvent was exchanged with fresh DMF at least three times within 12 h.

3. Results and discussions

3.1 Synthesis and structure description of NPF-320-RE

Tetratopic ligand **H₄L** was previously synthesized by our group and used for constructing the 4,8-c Zr-based NPF-320 with scu topology.[55] This success prompted us to explore the possibility

This journal is © The Royal Society of Chemistry 2024

J. Mater. Chem. C, 2024, **12**, 2836–2842 | **2837**

of its use to synthesize RE-MOFs with similar topology. Eddaoudi and co-workers have reported that H_4L_0, a structure prototype of H_4L can be used to produce a RE-MOF (*i.e.*, ftw-MOF-2) with 4,12-c **ftw** topology (Fig. 1a),[45] for which 2-fluorobenzoic acid (2-FBA) was used as the sole modulator. It is known that the nature and composition of the modulator used in Zr-MOF synthesis is critical for producing certain topologies. We thus hypothesized that a similar strategy can be adapted for the synthesis of RE-MOFs. Indeed, a solvothermal reaction between $Eu(NO_3)_3 \cdot 6H_2O$ and H_4L in the presence of 2-FBA for 48 h yielded colorless cubic block-shaped crystals (Fig. S3, ESI†), suggesting the formation of RE-MOFs with 4,12-c **ftw** topology, which is consistent with Eddaoudi's observation.[45] Interestingly, by introducing a co-modulator, trifluoroacetic acid (TFA), some needle-shaped crystals appeared in the product mixture (Fig. S3, ESI†). With careful adjustment of the amount of 2-FBA and TFA during the MOF synthesis, a single phase of needle-shaped crystals was obtained as NPF-320-Eu (Fig. 1b, c and Fig. S3, ESI†).

Single-crystal X-ray diffraction (sc-XRD) study reveals that NPF-320-Eu crystallizes in the orthorhombic crystal system with the *Cmmm* space group (Table S1, ESI†). In the framework of NPF-320-Eu, each ligand is coordinated to four Eu_6 clusters and each Eu_6 cluster is coordinated to eight ligands with four above and four below the equatorial plane, and eight terminal H_2O/OH^- groups in the equatorial plane (Fig. S4, ESI†), with the with the overall formula of $Eu_6(\mu_3\text{-}F)_8(H_2O/OH^-)_8(L)_2$. It should be noted that the presence of F^--containing clusters was further confirmed by, in addition to the better crystallographic refinement compared with OH- group, SEM/EDX mapping (Fig. S5, ESI†) and the ^{19}F NMR spectrum of an acid-digested sample (Fig. S6, ESI†). The connectivity of NPF-320-Eu belongs to a 4,8-c net, with the similar **scu** topology as NPF-300 and NPF-320.[7,55] It should be noted that the 4,8-c **scu** topology is rarely reported in RE-MOFs.[54,56] Due to the steric hindrance

caused by the two methyl groups, the three phenyl rings on the backbone of the primary ligand are not coplanar, with the dihedral angle of 60.3 °C (Fig. S7, ESI†). NPF-320-Eu features four large 1D open channels: three rhombic channels with the size of 27×15 Å along the *c* axis, 7×12 Å along the *b* axis, and 5×9 Å along the *a* axis, and one hexagonal channel with a diameter of 12 Å along *a* axis (Fig. S9, ESI†). NPF-320-Tb was synthesized using the same co-modulator strategy in an iso-structural form as NPF-320-Eu, which is confirmed by sc-XRD study (Table S1, ESI†). Powder X-ray diffraction (PXRD) patterns confirm the bulk phase purity of the as-synthesized NPF-320-RE when compared to the simulated patterns from the corresponding single-crystal structure (Fig. S13, ESI†).

3.2 Linkers installation in NPF-320-RE

We expect that NPF-320-RE MOFs that consist of 8-connected RE_6 clusters are ideal platforms for secondary linker installation *via* the replacement of H_2O/OH^- groups on the clusters according to the size matching principle.[55] In NPF-320-Eu, the pocket size along the *c* axis, defined as the O–O distance between the opposing H_2O/OH^- groups on the Eu_6 clusters, is 11.8 Å, and the pocket size along the *a* axis is 15.0 Å (Fig. 1d). These values are similar as those found in NPF-320,[55] which fit favorably with secondary linkers SL_1 (11.3 Å) and SL_2 (15.4 Å), respectively (Fig. 2).

We first tested the possible installation of SL_2. Briefly, as synthesized NPF-320-Eu single crystals were placed in the solution of SL_2 in DMF at 60 °C for 12 h, and the resulting single crystalline material, termed NPF-320-Eu-SL_2, belongs to the same *Cmmm* space group as NPF-320-Eu with the overall formula of $Eu_6(\mu_3\text{-}F)_8(H_2O/OH^-)_4(L)_2(SL_2)$ (Table S1, ESI†). As expected, in NPF-320-Eu-SL_2, each Eu_6 cluster is 10-connected to eight primary ligand **L** and two secondary linker SL_2 along the *a* axis. According to the crystal structure data, the molar
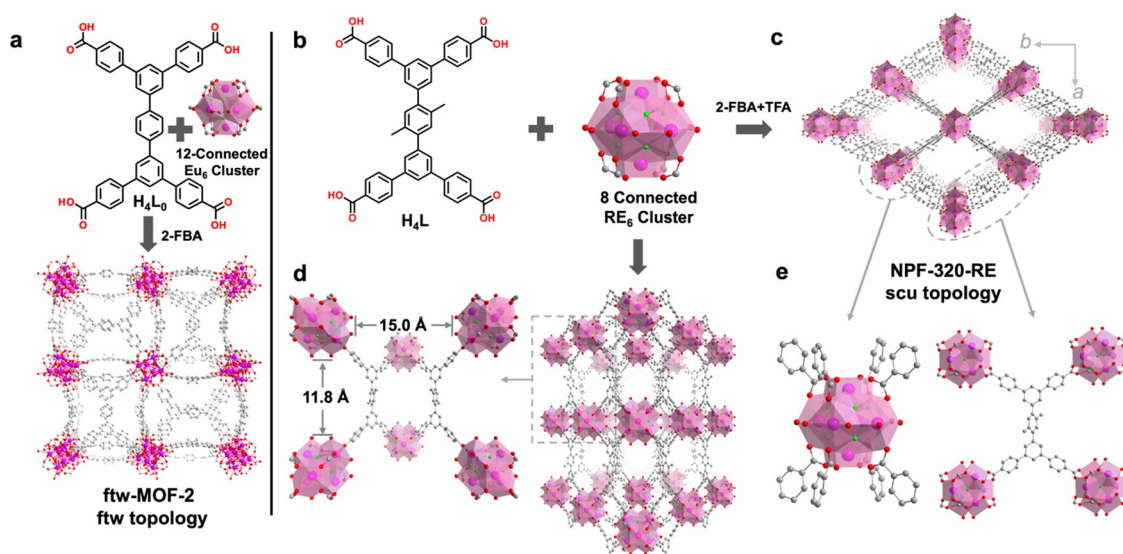

Fig. 1 (a) Formation of ftw-MOF-2 from the assembly of 12-connected Eu_6 cluster with ligand H_4L_0. (b) Primary ligand H_4L and 8-connected RE_6 cluster. (b) Topological representation of NPF-320-RE (C, gray; O, red; F, green; RE, pink polyhedron). (c) Simplified structure and (d) the two open pockets of NPF-320-Eu. (e) Connectivity of RE_6 cluster and ligand H_4L in NPF-320-RE.
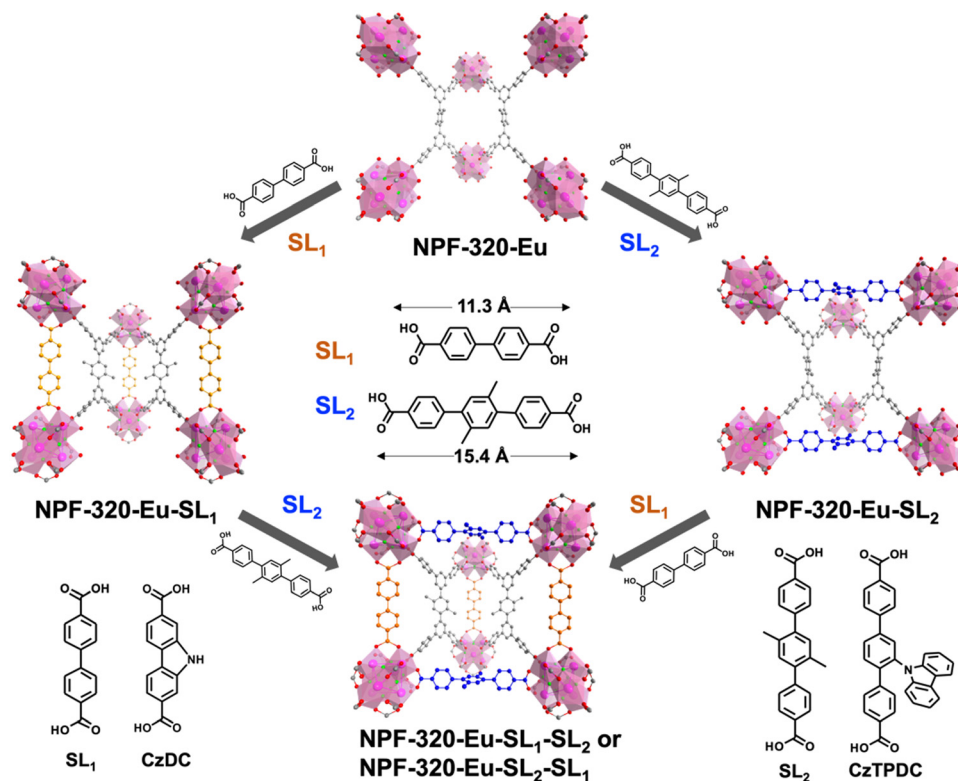
2838 | *J. Mater. Chem. C*, 2024, **12**, 2836–2842

This journal is © The Royal Society of Chemistry 2024

Fig. 2 Stepwise post-synthetic installation of secondary linkers in NPF-320-Eu.

ratio between primary ligand **L** and **SL₂** is 2 : 1, which is further confirmed by the ^{1}H NMR spectrum of an acid digested sample (Fig. S14, ESI†). Upon the successful installation of **SL₂**, the O–O distance between the opposing H_2O/OH^- groups on the Eu_6 clusters is 11.6 Å and does not change significantly. Thus, we next attempted to install **SL₁** into the open pockets along the c axis of NPF-320-Eu-**SL₂**, and the resulting crystalline materials, named NPF-320-Eu-**SL₂**–**SL₁**, crystallized in the same *Cmmm* space group and the presence of **SL₁** was observed along the c axis (Fig. 2 and Table S1, ESI†). In NPF-320-Eu-**SL₂**–**SL₁** each Eu_6 cluster is now 12-connected to eight primary ligand **L**, two **SL₁**, and two **SL₂**, which gives an overall formula of $Eu_6(\mu_3\text{-F})_8$ (**L**)₂(**SL₂**)(**SL₁**). Similarly, the molar ratio of **L**:**SL₂**:**SL₁** of 2 : 1:1 was also confirmed by ^{1}H NMR (Fig. S15, ESI†). The success of the linker installation on the bulk scale was further examined by PXRD patterns, which exhibit the similar peaks to the simulation (Fig. S16, ESI†).

We next attempted to install the secondary linkers into the open pockets of NPF-320-Eu *via* the alternate route, *i.e.*, first **SL₁** followed by **SL₂**. Indeed, single crystals of NPF-320-Eu-**SL₁** were obtained by heating NPF-320-Eu in a solution of **SL₁** in DMF (Fig. 2 and Table S1, ESI†), and the expected molar ratio of **L**:**SL₁** was supported by ^{1}H NMR spectrum of the acid digested sample (Fig. S17, ESI†). The subsequent installation of **SL₂** was also successful, resulting in NPF-320-Eu-**SL₁**–**SL₂** that has essentially the same structure of NPF-320-Eu-**SL₂**–**SL₁**, confirmed by PXRD (Fig. S16, ESI†). It should be noted that we also obtained a single crystalline material by installing 2,2′-bipyridine-5,

5′-dicarboxylic acid (bpy) into NPF-320-Eu (Table S1 and Fig. S18, ESI†). The versatile metal-binding ability of ligand **bpy** offers a vast future opportunity enrich the photophysical, catalytic, optical properties of NPF-320-RE materials.

3.3 Photosensitizer installation in NPF-320-RE

Having confirmed the success of the installation of two secondary linkers with different length into NPF-320-Eu, we next set out to use this strategy to enrich the functionalities of the RE-MOFs. One objective is to enhance the luminescent properties of NPF-320-RE by lowering the excitation energy. Since the primary ligand H_4**L** only absorb light in the UVB region (280–315 nm) (Fig. S19, ESI†), it is beneficial to red shift the excitation wavelength. In fact, many common MOF ligand do not strongly absorb light in the UVA (315–400 nm) or visible region (>400 nm), which limits their wider applications. Carbazole is a well-known electron donor and its derivatives have been widely used in optoelectronic and photocatalysis applications.[57] Thus, we envisioned that carbazole-containing ligand such as 9*H*-carbazole-2,7-dicarboxylic acid (**CzDC**) and carbazole-substituted terphenyl dicarboxylic acid (**CzTPDC**) (Fig. 2) should serve as good photosensitizers. More importantly, **CzDC** and **CzTPDC** have a similar length of **SL₁** and **SL₂** to be installed into the pockets along the c axis and a axis, respectively.

Indeed, upon excitation at 365 nm, **CzDC** and **CzTPDC** exhibit strong blue emissions with the λ_{max} at 400 nm and 460 nm, respectively (Fig. S20 and S21, ESI†), suggesting likely

This journal is © The Royal Society of Chemistry 2024

J. Mater. Chem. C, 2024, **12**, 2836–2842 | **2839**

good sensitizing capabilities to RE cations with different efficiencies. Installation of **CzDC** and **CzTPDC** into NPF-320-Eu and NPF-320-Tb were achieved by similar method described above. The successful linker installation was confirmed by ^{1}H NMR spectra of the corresponding acid digested NPF-320-Eu-**CzDC** and NPF-320-Eu-**CzTPDC** (Fig. S22 and S23, ESI†). PXRD patterns also indicate that the crystallinity of the materials retains after linker installation, and more importantly matches well with NPF-320-**SL$_1$** and NPF-320-**SL$_2$**, respectively (Fig. S24, ESI†).

After linker installation, both NPF-320-Eu-**CzDC** and NPF-320-Eu-**CzTPDC** display three relatively intense emissions at 589, 620, and 700 nm which are originated from the $^5D_0 \rightarrow {}^7F_J$ ($J = 1$, 2, and 4) transitions of Eu^{3+} ions (Fig. 3a–c). No apparent fluorescent emission based on the installed linker was observed, indicating a highly efficient energy transfer from the sensitizer to Eu. Moreover, to our delight, compared to the parent NPF-320-Eu, both ternary frameworks appear much brighter upon excitation at 365 nm (Fig. 3a–c, inset), with a slightly decrease of the luminescence lifetime from 1.62 ms in NPF-320-Eu to 1.52 ms and 1.47 ms in NPF-320-Eu-**CzDC** and NPF-320-Eu-**CzTPDC**, respectively (Fig. S25, ESI†).

In sharp contrast, the luminescence enhancement of NPF-320-Tb was only observed upon the installation of **CzDC**

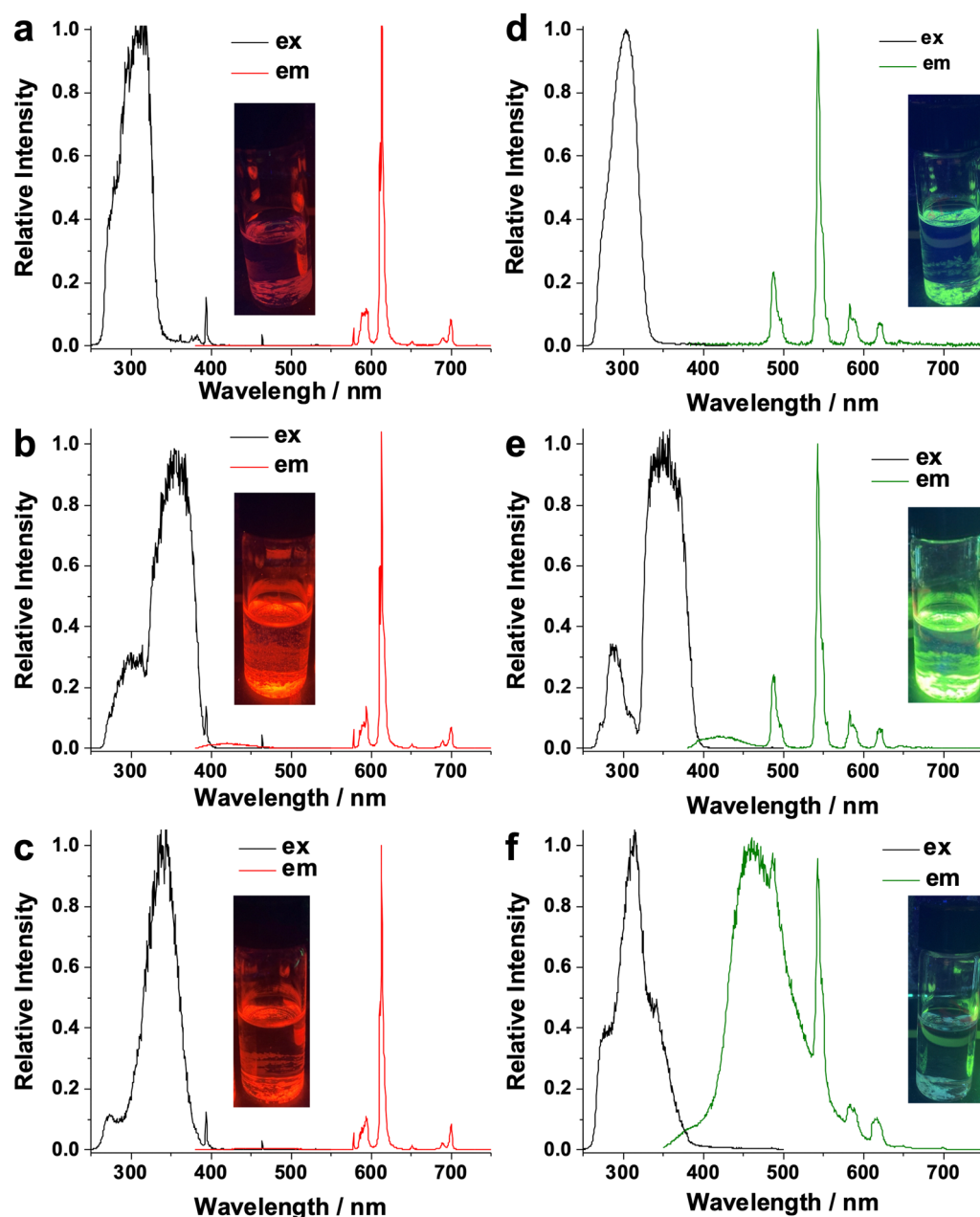Fig. 3 The excitation and emission spectra of (a) NPF-320-Eu, (b) NPF-320-Eu-**CzDC**, (c) NPF-320-Eu-**CzTPDC**, (d) NPF-320-Tb, (e) NPF-320-Tb-**CzDC**, (f) NPF-320-Tb-**CzTPDC**. Inset: The photograph under UV light (λ = 365 nm).

2840 | *J. Mater. Chem. C*, 2024, **12**, 2836–2842

This journal is © The Royal Society of Chemistry 2024

(Fig. 3e), which displays the emission peaks at 492, 542, 587, and 621 nm assigned to the $^5D_4 \rightarrow {}^7F_J$ ($J = 6, 5, 4,$ and 3) transitions of Tb^{3+} ions. In fact, the green emission from Tb^{3+} in NPF-320-Tb-**CzTPDC** was significantly quenched after the post-synthetic installation (Fig. 3f). At the same time, a weak, broad emission band around 460 nm attributed to **CzTPDC** is also detected, indicating the energy transfer is inefficient. This is likely due to the lower energy of the triplet state of **CzTPDC** compared to **CzDC**. Indeed, the phosphorescence spectrum of **CzTPDC** indicates a triplet state energy of $20\,964$ cm^{-1} (Fig. S26a, ESI†), which is lower than that of CzDC (Fig. S26b, ESI†) and only slightly higher than the $^5D_4$ excited state of Tb^{3+} ($20\,408$ cm^{-1}), less than the empirical optimum gap of 1850 cm^{-1} for the efficient energy transfer.[58] In fact, the decreased Tb^{3+} lifetime (0.74 ms) in NPF-320-Tb-**CzTPDC** compared to 1.09 ms of NPF-320-Tb-**CzDC** also suggested a back energy transfer pathway from Tb^{3+} to ligand triplet state. This energy relaxation route further deteriorates the energy transfer process from the primary ligand to Tb, indicated by a weaker green luminescence in NPF-320-Tb-**CzTPDC** compared to NPF-320-Tb (Fig. 3d and f). Overall, our work exemplifies the power of the stepwise linker installation strategy to diversify the photoluminescent properties of RE-MOFs. A promotion or inhibition of energy transfer process with RE ions, secondary linker, as well as the primary ligand can be precisely controlled by judicious choice the photosensitizers.

4. Conclusion

In conclusion, we report a new synthesis strategy for preparing RE-MOFs consisting of less connected RE$_6$ clusters for post-synthetic linker installation. Previous synthesis of RE-MOFs using square or rectangular tetratopic ligands usually results in the formation of 12-connected RE$_6$ clusters with underlying **ftw** or **shp** topology which inhibit further linker installation and functionality incorporation. Herein, by using a co-modulator strategy, namely, a mixture of TFA as a second modulator combined with a commonly used 2-FBA, we have successfully used a rectangular linker to prepare RE-MOFs that consist of 8-connected RE$_6$ clusters with underlying **scu** topology. More interestingly, the eight connected RE$_6$ clusters in the **scu** network enable the precise installation of secondary linkers along the *a* and *c* axis *via* single-crystal-to-single-crystal transformation. Moreover, two photosensitizer-based secondary linkers (**CzDC** and **CzTPDC**) were successfully installed in NPF-320-RE and govern the energy transfer processes between the primary/secondary ligands with the RE ions. To the best of our knowledge, this is the first example of the installation of two distinct secondary linkers within a RE-MOF, which paves a versatile way for the future design multifunctional RE-MOFs.

Conflicts of interest

There are no conflicts to declare.

Acknowledgements

References

1 M. Eddaoudi, D. B. Moler, H. Li, B. Chen, T. M. Reineke, M. O'Keeffe and O. M. Yaghi, *Acc. Chem. Res.*, 2001, **34**, 319–330.

2 M. J. Kalmutzki, N. Hanikel and O. M. Yaghi, *Sci. Adv.*, 2018, **4**, eaat9180.

3 Y. Bai, Y. Dou, L. H. Xie, W. Rutledge, J. R. Li and H. C. Zhou, *Chem. Soc. Rev.*, 2016, **45**, 2327–2367.

4 S. Yuan, L. Feng, K. Wang, J. Pang, M. Bosch, C. Lollar, Y. Sun, J. Qin, X. Yang, P. Zhang, Q. Wang, L. Zou, Y. Zhang, L. Zhang, Y. Fang, J. Li and H. C. Zhou, *Adv. Mater.*, 2018, **30**, 1704303.

5 S. Yuan, W. Lu, Y. P. Chen, Q. Zhang, T. F. Liu, D. Feng, X. Wang, J. Qin and H. C. Zhou, *J. Am. Chem. Soc.*, 2015, **137**, 3177–3180.

6 C. X. Chen, Z. Wei, J. J. Jiang, Y. Z. Fan, S. P. Zheng, C. C. Cao, Y. H. Li, D. Fenske and C. Y. Su, *Angew. Chem., Int. Ed.*, 2016, **55**, 9932–9936.

7 X. Zhang, B. L. Frey, Y. S. Chen and J. Zhang, *J. Am. Chem. Soc.*, 2018, **140**, 7710–7715.

8 T. M. Reineke, M. Eddaoudi, M. O'Keeffe and O. M. Yaghi, *Angew. Chem., Int. Ed.*, 1999, **38**, 2590–2594.

9 T. M. Reineke, M. Eddaoudi, M. Fehr, D. Kelley and O. M. Yaghi, *J. Am. Chem. Soc.*, 1999, **121**, 1651–1657.

10 J. Rocha, L. D. Carlos, F. A. Paz and D. Ananias, *Chem. Soc. Rev.*, 2011, **40**, 926–940.

11 Y. Cui, Y. Yue, G. Qian and B. Chen, *Chem. Rev.*, 2012, **112**, 1126–1162.

12 C. Pagis, M. Ferbinteanu, G. Rothenberg and S. Tanase, *ACS Catal.*, 2016, **6**, 6063–6072.

13 B. Yan, *Acc. Chem. Res.*, 2017, **50**, 2789–2798.

14 E. A. Dolgopolova, A. M. Rice, C. R. Martin and N. B. Shustova, *Chem. Soc. Rev.*, 2018, **47**, 4710–4728.

15 S. Wu, H. Min, W. Shi and P. Cheng, *Adv. Mater.*, 2020, **32**, 1805871.

16 F. Saraci, V. Quezada-Novoa, P. R. Donnarumma and A. J. Howarth, *Chem. Soc. Rev.*, 2020, **49**, 7949–7977.

17 J. C. Bunzli and C. Piguet, *Chem. Rev.*, 2002, **102**, 1897–1928.

18 D. X. Xue, A. J. Cairns, Y. Belmabkhout, L. Wojtas, Y. Liu, M. H. Alkordi and M. Eddaoudi, *J. Am. Chem. Soc.*, 2013, **135**, 7660–7667.

19 D. X. Xue, Y. Belmabkhout, O. Shekhah, H. Jiang, K. Adil, A. J. Cairns and M. Eddaoudi, *J. Am. Chem. Soc.*, 2015, **137**, 5034–5040.

20 Z. Chen, L. J. Weselinski, K. Adil, Y. Belmabkhout, A. Shkurenko, H. Jiang, P. M. Bhatt, V. Guillerm, E. Dauzon, D. X. Xue, M. O'Keeffe and M. Eddaoudi, *J. Am. Chem. Soc.*, 2017, **139**, 3265–3274.

This journal is © The Royal Society of Chemistry 2024

J. Mater. Chem. C, 2024, **12**, 2836–2842 | **2841**

21 T. Y. Luo, C. Liu, S. V. Eliseeva, P. F. Muldoon, S. Petoud and N. L. Rosi, *J. Am. Chem. Soc.*, 2017, **139**, 9333–9340.

22 D. Alezi, A. M. Peedikakkal, L. J. Weselinski, V. Guillerm, Y. Belmabkhout, A. J. Cairns, Z. Chen, L. Wojtas and M. Eddaoudi, *J. Am. Chem. Soc.*, 2015, **137**, 5421–5430.

23 L. Zhang, S. Yuan, L. Feng, B. Guo, J. S. Qin, B. Xu, C. Lollar, D. Sun and H. C. Zhou, *Angew. Chem., Int. Ed.*, 2018, **57**, 5095–5099.

24 L. Feng, J. Pang, P. She, J. L. Li, J. S. Qin, D. Y. Du and H. C. Zhou, *Adv. Mater.*, 2020, **32**, 2004414.

25 Y. Wang, L. Feng, W. Fan, K. Y. Wang, X. Wang, X. Wang, K. Zhang, X. Zhang, F. Dai, D. Sun and H. C. Zhou, *J. Am. Chem. Soc.*, 2019, **141**, 6967–6975.

26 B. Guo, H. Liu, J. Pang, Q. Lyu, Y. Wang, W. Fan, X. Lu and D. Sun, *J. Hazard. Mater.*, 2022, **436**, 129094.

27 F. Li, K. Y. Wang, Z. Liu, Z. Han, D. Kuai, W. Fan, L. Feng, Y. Wang, X. Wang, Y. Li, Z. Yang, R. Wang, D. Sun and H. C. Zhou, *JACS Au*, 2023, **3**, 1337–1347.

28 J. P. Vizuet, M. L. Mortensen, A. L. Lewis, M. A. Wunch, H. R. Firouzi, G. T. McCandless and K. J. Balkus, Jr., *J. Am. Chem. Soc.*, 2021, **143**, 17995–18000.

29 M. S. Christian, K. J. Fritzsching, J. A. Harvey, D. F. Sava Gallis, T. M. Nenoff and J. M. Rimsza, *JACS Au*, 2022, **2**, 1889–1898.

30 S. Yuan, Y. P. Chen, J. S. Qin, W. Lu, L. Zou, Q. Zhang, X. Wang, X. Sun and H. C. Zhou, *J. Am. Chem. Soc.*, 2016, **138**, 8912–8919.

31 S. Yuan, L. Zou, H. Li, Y. P. Chen, J. Qin, Q. Zhang, W. Lu, M. B. Hall and H. C. Zhou, *Angew. Chem., Int. Ed.*, 2016, **55**, 10776–10780.

32 C. X. Chen, Z. W. Wei, J. J. Jiang, S. P. Zheng, H. P. Wang, Q. F. Qiu, C. C. Cao, D. Fenske and C. Y. Su, *J. Am. Chem. Soc.*, 2017, **139**, 6034–6037.

33 C. X. Chen, Q. F. Qiu, C. C. Cao, M. Pan, H. P. Wang, J. J. Jiang, Z. W. Wei, K. Zhu, G. Li and C. Y. Su, *Chem. Commun.*, 2017, **53**, 11403–11406.

34 S. Yuan, P. Zhang, L. Zhang, A. T. Garcia-Esparza, D. Sokaras, J. S. Qin, L. Feng, G. S. Day, W. Chen, H. F. Drake, P. Elumalai, S. T. Madrahimov, D. Sun and H. C. Zhou, *J. Am. Chem. Soc.*, 2018, **140**, 10814–10819.

35 C. X. Chen, Q. F. Qiu, M. Pan, C. C. Cao, N. X. Zhu, H. P. Wang, J. J. Jiang, Z. W. Wei and C. Y. Su, *Chem. Commun.*, 2018, **54**, 13666–13669.

36 J. Pang, S. Yuan, J. Qin, M. Wu, C. T. Lollar, J. Li, N. Huang, B. Li, P. Zhang and H. C. Zhou, *J. Am. Chem. Soc.*, 2018, **140**, 12328–12332.

37 C. C. Cao, C. X. Chen, Z. W. Wei, Q. F. Qiu, N. X. Zhu, Y. Y. Xiong, J. J. Jiang, D. Wang and C. Y. Su, *J. Am. Chem. Soc.*, 2019, **141**, 2589–2593.

38 W. Morris, B. Volosskiy, S. Demir, F. Gándara, P. L. McGrier, H. Furukawa, D. Cascio, J. F. Stoddart and O. M. Yaghi, *Inorg. Chem.*, 2012, **51**, 6443–6445.

39 O. V. Gutov, W. Bury, D. A. Gomez-Gualdron, V. Krungleviciute, D. Fairen-Jimenez, J. E. Mondloch, A. A. Sarjeant, S. S. Al-Juaid, R. Q. Snurr, J. T. Hupp, T. Yildirim and O. K. Farha, *Chem. – Eur. J.*, 2014, **20**, 12389–12393.

40 Z. Wei, Z. Y. Gu, R. K. Arvapally, Y. P. Chen, R. N. McDougald, Jr., J. F. Ivy, A. A. Yakovenko, D. Feng, M. A. Omary and H. C. Zhou, *J. Am. Chem. Soc.*, 2014, **136**, 8269–8276.

41 D. Feng, Z. Y. Gu, Y. P. Chen, J. Park, Z. Wei, Y. Sun, M. Bosch, S. Yuan and H. C. Zhou, *J. Am. Chem. Soc.*, 2014, **136**, 17714–17717.

42 T. C. Wang, W. Bury, D. A. Gómez-Gualdrón, N. A. Vermeulen, J. E. Mondloch, P. Deria, K. Zhang, P. Z. Moghadam, A. A. Sarjeant, R. Q. Snurr, J. F. Stoddart, J. T. Hupp and O. K. Farha, *J. Am. Chem. Soc.*, 2015, **137**, 3585–3591.

43 T. F. Liu, D. Feng, Y. P. Chen, L. Zou, M. Bosch, S. Yuan, Z. Wei, S. Fordham, K. Wang and H. C. Zhou, *J. Am. Chem. Soc.*, 2015, **137**, 413–419.

44 S. B. Kalidindi, S. Nayak, M. E. Briggs, S. Jansat, A. P. Katsoulidis, G. J. Miller, J. E. Warren, D. Antypov, F. Cora, B. Slater, M. R. Prestly, C. Marti-Gastaldo and M. J. Rosseinsky, *Angew. Chem., Int. Ed.*, 2015, **54**, 221–226.

45 R. Luebke, Y. Belmabkhout, L. J. Weselinski, A. J. Cairns, M. Alkordi, G. Norton, L. Wojtas, K. Adil and M. Eddaoudi, *Chem. Sci.*, 2015, **6**, 4095–4102.

46 R. G. AbdulHalim, P. M. Bhatt, Y. Belmabkhout, A. Shkurenko, K. Adil, L. J. Barbour and M. Eddaoudi, *J. Am. Chem. Soc.*, 2017, **139**, 10715–10722.

47 H. Wang, X. Dong, V. Colombo, Q. Wang, Y. Liu, W. Liu, X. L. Wang, X. Y. Huang, D. M. Proserpio, A. Sironi, Y. Han and J. Li, *Adv. Mater.*, 2018, **30**, 1805088.

48 D. X. Xue, A. Cadiau, L. J. Weselinski, H. Jiang, P. M. Bhatt, A. Shkurenko, L. Wojtas, Z. Chen, Y. Belmabkhout, K. Adil and M. Eddaoudi, *Chem. Commun.*, 2018, **54**, 6404–6407.

49 V. Guillerm, L. J. Weselinski, Y. Belmabkhout, A. J. Cairns, V. D'Elia, L. Wojtas, K. Adil and M. Eddaoudi, *Nat. Chem.*, 2014, **6**, 673–680.

50 H. Jiang, J. Jia, A. Shkurenko, Z. Chen, K. Adil, Y. Belmabkhout, L. J. Weselinski, A. H. Assen, D. X. Xue, M. O'Keeffe and M. Eddaoudi, *J. Am. Chem. Soc.*, 2018, **140**, 8858–8867.

51 S. Roy, A. Chakraborty and T. K. Maji, *Coord. Chem. Rev.*, 2014, **273–274**, 139–164.

52 G. K. Angeli, D. Batzavali, K. Mavronasou, C. Tsangarakis, T. Stuerzer, H. Ott and P. N. Trikalitis, *J. Am. Chem. Soc.*, 2020, **142**, 15986–15994.

53 G. K. Angeli, E. Loukopoulos, K. Kouvidis, A. Bosveli, C. Tsangarakis, E. Tylianakis, G. Froudakis and P. N. Trikalitis, *J. Am. Chem. Soc.*, 2021, **143**, 10250–10260.

54 X. L. Lv, L. Feng, L. H. Xie, T. He, W. Wu, K. Y. Wang, G. Si, B. Wang, J. R. Li and H. C. Zhou, *J. Am. Chem. Soc.*, 2021, **143**, 2784–2791.

55 Y. Hu, X. Zhang, R. S. H. Khoo, C. Fiankor, X. Zhang and J. Zhang, *J. Am. Chem. Soc.*, 2023, **145**, 13929–13937.

56 H. L. Xia, K. Zhou, J. Guo, J. Zhang, X. Huang, D. Luo, X. Y. Liu and J. Li, *Chem. Sci.*, 2022, **13**, 9321–9328.

57 A. van Dijken, J. J. Bastiaansen, N. M. Kiggen, B. M. Langeveld, C. Rothe, A. Monkman, I. Bach, P. Stössel and K. Brunner, *J. Am. Chem. Soc.*, 2004, **126**, 7718–7727.

58 M. Latva, H. Takalo, V.-M. Mukkala, C. Matachescu, J. C. Rodríguez-Ubis and J. Kankare, *J. Lumin.*, 1997, **75**, 149–169.